IJREB

ISSN **2321-743X**

International Journal of Research in

Engineering and Bioscience

Volume **7** Issue **1** (Pages 61- 78)

Journal home page: www.ijreb.org

SYNTHESIS AND INVESTIGATION ON STRUCTURAL, OPTICAL, MECHANICAL AND SECOND – ORDER NON – LINEAR OPTICAL PROPERTIES OF PURE AND L – HISTIDINE DOPED COPPER SULPHATE SINGLE CRYSTALS

M. Mary Anne [1,3], M. Daniel Sweetlin [2,3]

1.Physics Research Centre, St. John's College, Palayamkottai, Tirunelveli 627002, India

[2] Department of Physics, St. John's College, Palayamkottai, Tirunelveli 627002, India

[3] Affiliated to Manonmaniam Sundaranar University, Abishekapatti, Tirunelveli 627012, India

Corresponding author:gosiksanthi@gmail.com

ABSTRACT

Optical high quality semi-organic pure and L – Histidine doped Copper Sulphate single crystals were grown by slow evaporation technique. The crystallographic system and lattice parameters were determined by powder X-Ray Diffraction analysis which designates that the synthesized crystals belong to triclinic system crystallising in space group *P1*. The optical characteristics of the single crystals were analyzed by the UV-Vis NIR spectral analysis and the band gap energy, lower cut-off wavelength, percentage of transmittance end the refractive index of the materials have been calculated. The interaction of characteristic functional groups was validated by Fourier Transform Infrared (FTIR) spectral analysis. The mechanical strength and the mechanical factors of the grown crystals were estimated by employing Vickers micro hardness test. The second order nonlinear optical properties of the crystals were computed using Q switched High Energy Nd: YAG Laser.

KEYWORDS

Single Crystals, Slow Evaporation Technique, Optical Transmittance, powder X-ray Diffraction analysis, UV-Vis NIR analysis, FTIR analysis, Vickers micro hardness test, Second Harmonic Generation (SHG).

INTRODUCTION

In recent years, a lot of attention has been drawn towards the growth of novel nonlinear optical materials due to their extensive range of applications in the field of engineering and biology. Transmission of data has observed an exponential growth in the past twenty years. Optically tuneable crystals adorn the laser and photonic industries as energy harvesters. It is predicted that around 1 billion Gigabytes of data is transmitted every day. The industry will highly benefit with the preface of nonlinear optical materials as a substitute for regular cables. There is a great potential for nonlinear optical materials with high optical and structural property due to the progress of optical communication system [1–5]. Organic molecular materials have drawn augmented interest due to the sole viewpoints for fundamental research and realistic applications. In recent years, the material industries have been exploring for novel nonlinear optical materials. Organic nonlinear optical (NLO)

materials are used in optical data storage technologies, laser technologies, transistors, conductors, electro-optic modulators, electronic materials, optical circuits, optical communication, light-emitting diodes, optical signal processing, colour displays, frequency doubling, integrated optics, photonic applications and electro-optic switches [6–9] .

Organic materials have excellent chemical flexibility, optical nonlinearity, thermal stability and outstanding transmittance in the UV–visible regions. The optical properties of materials

should be studied to verify their fittingness for optoelectronic, photovoltaic applications and devices [10].

Amino acids are bi-functional organic compounds which include both carboxylic acid (COOH) and amino group (NH_2) recognized as zwitterions that form hydrogen bonds. This hydrogen bonding takes part in a key factor in the formation of new organic materials with unexpected NLO and electro-optic properties [11, 12]. L- Histidine salts have attained important attention not only due to their unique parcels but also for possible operations to photonic and optoelectronic bias [13]. The anhydrous type of copper sulphate is a ashen green or gray-white powder. But its pentahydrate ($CuSO_4 \cdot 5H_2O$) form is bright blue in colour. Copper sulphate exothermically dissolves in water to supply the aquo complex $[Cu(H_2O)_6]^{2+}$ which has octahedral molecular geometry and is paramagnetic. Other names for Copper sulphates are copper (II) sulphate, bluestone and blue vitriol. These crystals are valuable for nonlinear optical devices based on their optical second harmonic generation. The NLO property of glycine affixed copper sulphate single crystal was reported by S.N. Jeyanthi etal. very recently [14]. In the present study, the grown crystals are subjected to powder XRD analysis, FTIR analysis, UV-Vis-NIR analysis,

micro hardness studies and second harmonic generation test.

2 Experimental Procedure

Analytic Reagent (AR) grade copper sulphate salt was made use for the growth of pure and L-Histidine doped copper sulphate single crystals. Accordance to the solubility test, appropriate amount of copper sulphate salt was measured. Copper sulphate salt was mixed with deionised water and the mixture was kept on a magnetic stirrer and stirred well by applying mild temperature about 40˚C for about 3 hours. Stirring was done for a long time for the homogenous mixing of the mixture. In the solution growth technique, selection of a solvent which is reasonably soluble takes part a vital role. For doping purpose 0.006 wt% L-Histidine was mixed with the same solution. Then the solution was finely covered with a plane thin paper sheet. Good quality transparent crystals were synthesized within 10-15 days. The synthesized crystals were carried out powder X-ray diffraction, Fourier Transform Infrared analysis, UV-Visible spectral analysis, micro hardness studies and second harmonic generation test. Transparent high-quality crystals with perfect shape and free from macro defects were used for characterization. The reaction between H_2O and $CuSO_4$ is represented as follows

$$CuSO_4\,(s) + 5H_2O\,(l) \rightarrow CuSO_4.5H_2O\,(s)$$

Copper sulphate Water Copper sulphate pentahydrate

The data sheet of pure and L-Histidine doped CS single crystals are given in Table 1.

Table 1 Data sheet of copper sulphate and L-Histidine

Compound	Formula	Molecular Mass (g/mol)	Density (g/cm^3)	PH at 100 g/l	Melting point (° C)	Water solubility (g/l)
Copper sulphate	$CuSO_4$	159.609	3.6	4-5	110	25
L-Histidine	$C_6H_9N_3O_2$	155.15	1.449	3.5-4.5	285	149.55

Fig. 1 and Fig. 2 are the photographs of pure and 0.006 wt% L-Histidine doped Copper sulphate (CS) single crystals respectively.

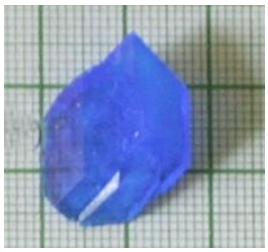

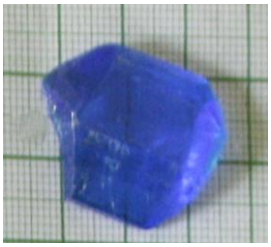

Fig. 1 Pure CS single crystal

Fig. 2 0.006 wt% L-Histidine doped CS single crystal

3 Result and discussion

3.1Powder X- Ray Diffraction Analysis

Powder X-ray diffraction analysis is applied for determining the crystalline nature of the grown crystals. It also enables to assess the assorted structure correlated parameters of the sampled material [15]. The powder XRD patterns of the grown pure and L-Histidine doped crystals were traced using monochromatic CuKα-1 radiation of wavelength 1.54060 Å within 2θ ranging from 10˚ to 80˚ at the rate 1° min^{-1} at temperature 25° C [16]. The different planes of reflections noticed in XRD patterns of pure and doped CS single crystals were indexed by INDEX software and are revealed in Fig. 3 and Fig. 4 respectively. It is scrutinized that the viewed XRD peaks at 2θ are at18.80˚, 22.3˚, 23.96˚, 29.11˚, 31.79˚, 35.07˚, 45.79˚, 60.41˚ and 66.17˚ belonging to the planes (111), (021), (021), (031), (200), (-140), (-242), (321) and (-140) for pure CS crystal and at15.92˚, 18.8˚, 22.5˚, 24.16˚, 25.18˚, 31.79˚, 32.39˚, 44.75˚ and 51.75˚ belonging to the planes (-110), (110), (021), (0-21), (120), (221), (130), (230) and (252) for doped CS crystal respectively[17]. The powder XRD diffraction data and the attained indexed (h k l) peaks were well matched with the JCPDS files [18]. The well-defined Bragg's peaks at specific 2θ angles show the high crystalline of the synthesized crystals. The pointed peaks created in the spectra prove high-quality crystalline of the cultivated single crystals [19]. The addition of the doping in the masterpiece of copper sulphate crystal improves the intensity of peaks compared to that of pure copper sulphate crystal. This reveals that the doping has brought a change in the internal structure of the crystal [20]. The highest peaks appear at 2θ~ 23.96˚ for pure CS crystal and 2θ~ 32.39˚ for the doped CS crystal and those refer to (021) and (130) planes respectively. These distinctions occur due to the shapes and colours of the crystals [21].

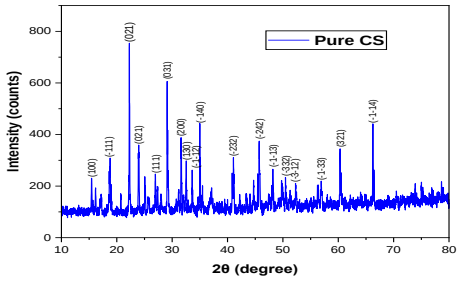

Fig. 3. Powder XRD spectrum of pure CS single crystal.

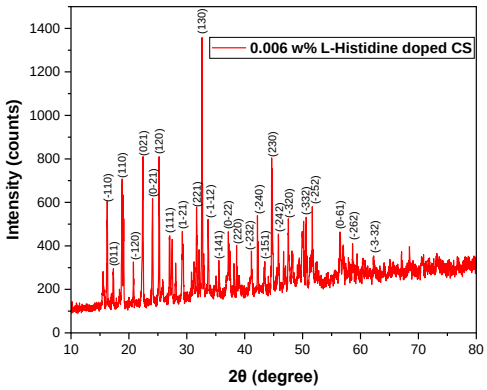

Fig. 4. Powder XRD spectrum of doped CS single crystal.

From the XRD data, it is monitored that the pure and doped CS crystals crystallize in triclinic crystal system with space group P1.The values of the lattice parameters are in excellent

agreement with the data reported previously [22]. The lattice parameters of the synthesized pure and doped CS crystals are tabulated in Table 2. There are several reasons for alterations in the lattice parameter such as stress, strain, defects, and changes in imperfections in the crystal lattice. Also, the increase in lattice parameters shows that the compressive stresses get produced in the crystal during the growth process [23].

Table 2 Lattice parameters of pure and doped CS single crystals

Parameters	Pure CS	L-Histidine doped CS
a (A˚)	6.121	6.118
b (A˚)	10.678	10.692
c (A˚)	5.931	5.953
α (º)	81.82	81.21
β (º)	107.41	107.32
γ (º)	102.41	102.81
Space group	P1	P1
Crystal system	Triclinic	Triclinic
Prominent peak at 2θ (degree)	22.3˚	32.39˚

3.2 Fourier Transform Infrared (FTIR) Analysis

The infrared spectral analysis is conceded to identify with the chemical bonding and it affords valuable information about the molecular structure of the compound [24]. The functional groups of the grown pure and doped CS crystals can be identified by carrying out FTIR analysis. The FTIR spectra were examined by using a *FTIR – 8400S* Fourier Transform Infrared spectrophotometer (SHIMADZU) between the range *500 cm^{-1}* and *4000 cm^{-1}*. The traced FTIR spectra of the pure and doped crystals are indicated in Fig. 5 and Fig. 6 respectively.

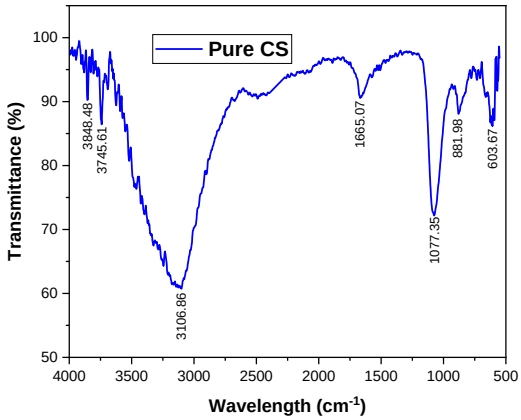

Fig. 5. FTIR spectrum of pure CS single crystal.

In the FTIR pattern of pure CS crystal, O-H stretching absorption band is identified at 3106.86 cm^{-1} [25]. Bending vibration of O-H becomes visible at 1665.07 cm^{-1} [26]. The Stretching vibration of S-O group is monitored at 1077.35 cm^{-1} [27]. The Vibration mode of metal ion Cu^{+2} (Cu-O-H) is observed at 881.98 cm^{-1}. The bending vibration mode of S-O group is found at 603.67 cm^{-1} [28]. For L – Histidine doped CS single crystal, O-H stretching absorption band is shifted at 3178.63 cm^{-1}. The shifting of bending vibration of O-H is noticed at

1675.44 cm^{-1}. The Stretching vibration of S-O group is recognized at 1077.35 cm^{-1}. The Vibration mode of metal ion Cu^{+2} (Cu-O-H) is shifted at 871.61 cm^{-1}. The shifting of bending vibration mode of S-O group is observed at 614.03 cm^{-1}. Analogous annotations were formerly reported by F. A. Miller and C. H. Wilkins for AR grade copper sulphate salt [29]. The distinction in manifestation of modes of ions (SO_4^{-2}) is pointed out to the chemical reactivity of copper salts on KBr windows [30]. The IR bands of the grown pure and doped CS crystals are tabulated in Table 3. From Table 2, it is obviously noticed that all bands shift to higher or lower wave numbers and this can be due to the external factors such that impurities, pressure and temperature during the growth of crystals [31].

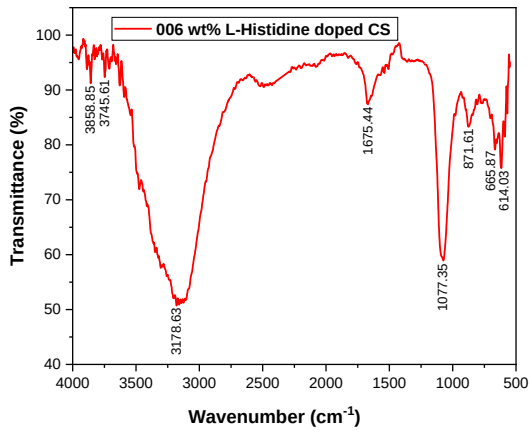

Fig. 6. FTIR spectrum of doped CS single crystal.

3.3 UV-Vis-NIR analysis

Organic nonlinear optical single crystals are largely used in optical applications where transparency, optical transmission range and cut-off wavelength are fundamental contemplations [32, 33]. Learning the optical properties of materials is important to assess the application of these materials in photovoltaic, optical data storage, optoelectronics and optical devices [34]. Optical studies provides valuable information about the molecular structure. It is also useful in calculating the energy of activation due to electronic excitation determining the fundamental bonding which is present in the materials [35]. Pharmaspec UV – 1700 UV – Visible Spectrophotometer (SHIMADZU) is used to record UV – visible spectra of pure and L-Histidine doped CS single crystals with a light source of wavelength of 366 nm in the wavelength range between 200 nm and 800 nm. Optical data was recorded for the pure and doped CS single crystals of thickness 10 mm and 7 mm

Table 3: IR bands of pure and L-Histidine doped CS single crystals

Wave number (cm^1)		Assignment
Pure CS	**L-Histidine doped CS**	
3106.86 cm^{-1}	3178.63 cm^{-1}	O-H stretching
1665.07 cm^{-1}	1675.44 cm^{-1}	O-H bending
1077.35 cm^{-1}	1077.35 cm^{-1}	S-O Stretching
881.98 cm^{-1}	871.61 cm^{-1}	Cu-O-H Vibration mode
603.67 cm^{-1}	614.03 cm^{-1}	S-O bending

respectively [36]. The recorded spectra of optical absorbance are illustrated in Fig. 7. The absorption coefficient was evaluated from the following relation

$$\alpha = \frac{2.303A}{t}$$

(1)

Here A is the absorbance and t is the thickness of the sample. The recorded transmittance spectra of the pure and doped single crystals are depicted in the range of 190 – 810 nm as shown in Fig. 8. From the plots, it is clearly noticed that the cut-off wavelengths are around 273.9 nm and 279.2 nm for pure and doped CS crystals respectively and the synthesized CS single crystals have excellent transmittance in the visible and near-IR regions. Band gap energy can be obtained from Tauc's plot and in order to compute the optical band gap, a plot of $(\alpha hv)^2$ versus hν is drawn and extrapolate the linear portion of the curves until they block the photon energy axis. The band gap energies are found to be 4.01 eV and 4.3 eV for pure and doped CS crystals respectively. Fig. 9 indicates Tauc's plots of pure and doped CS single crystals [37]. The performance of material depends mainly on the optical behaviour that outlines a basis for estimating its application in optoelectronic devices [38]. The extinction coefficient and refractive index are named as optical constants. The part of light loss is identified by extinction coefficient (K) of the material. The extinction coefficient is calculated using the following formula

$$K = \frac{\lambda\alpha}{4\pi}$$

(2)

here λ indicates the wavelength of the incident radiation. A graph of extinction coefficient versus wavelength is plotted in Fig. 10. The extinction coefficients of the synthesized pure and doped CS crystals have been noted to decrease with the rise in wavelength in the UV region and increase slightly in the visible region. It may be because of scattering efficiency, absorption and the nature of the scattering centres [39]. Its magnitude is of the order of 10^{-5}, which denotes that the material is less absorbed. The low value of the extinction coefficient points out the possibility for using the CS crystals for solar non-linear optical systems and thermal devices [40, 41].

The reflectance (R) and refractive index (n) of the grown CS crystals can be calculated from the following relations

$$R = \frac{\exp(-\alpha t) \pm \sqrt{\exp(-\alpha t)T - \exp(-3\alpha t)T + \exp(-2\alpha t)T^2}}{\exp(-\alpha t) + \exp(-2\alpha t)T}$$

(3)

$$n = \frac{1}{\mathrm{T}} + \left(\frac{1}{\mathrm{T}} - 1\right)^{1/2}$$

(4)

The optical and electrical conductivity are calculated using the formulae

$$\sigma_{op} = \frac{\alpha nc}{4\pi}$$

(5)

$$\sigma_{ele} = \frac{2\lambda\sigma_{op}}{\alpha}$$

(6)

Where *c* is the speed of light which is equal to 3 x 10^8 m/s. The skin depth (δ) is mathematically defined as

$$\delta = \frac{1}{\alpha} \quad (7)$$

The graph drawn for the skin depth versus wavelength for the pure and doped CS single crystals is revealed in Fig. 11. The figure shows that the skin depth decreases while moving towards high wavelength regions [42].

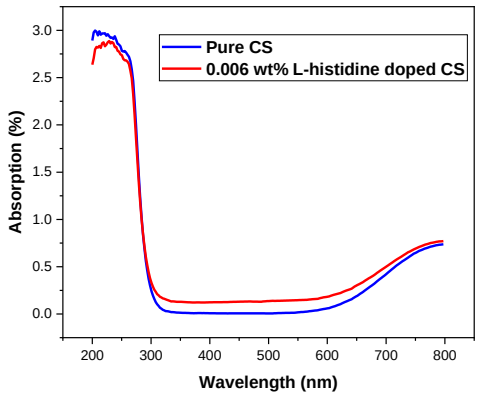

Fig. 7. UV-Vis-NIR absorbance spectra of pure and doped CS crystals.

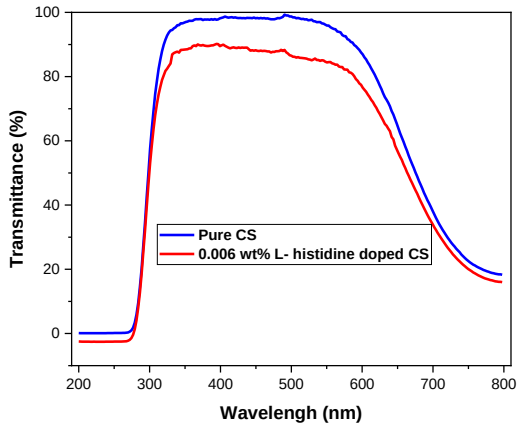

Fig. 8. UV-Vis-NIR transmittance spectra of pure and doped CS crystals.

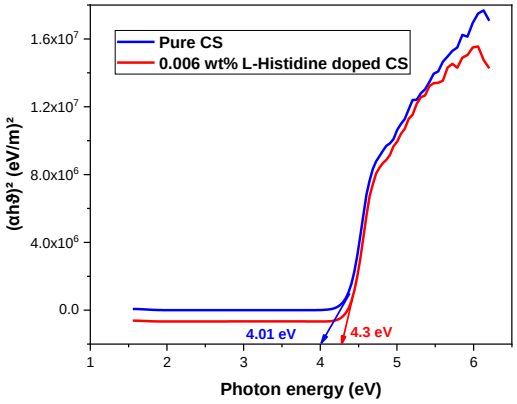

Fig. 9. Tauc's plot of pure and doped CS crystals.

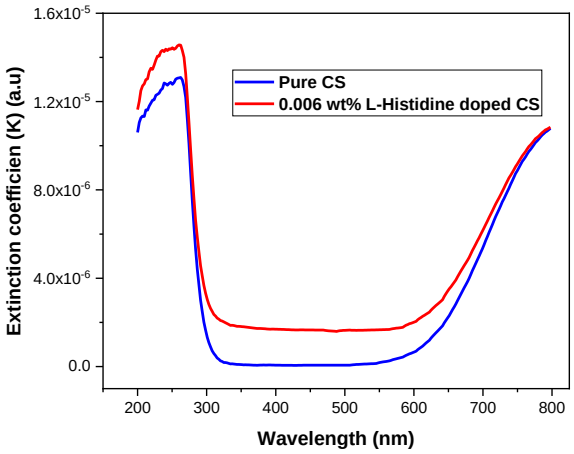

Fig. 10. Variation of extinction coefficient as a function of wavelength of pure and doped CS crystals.

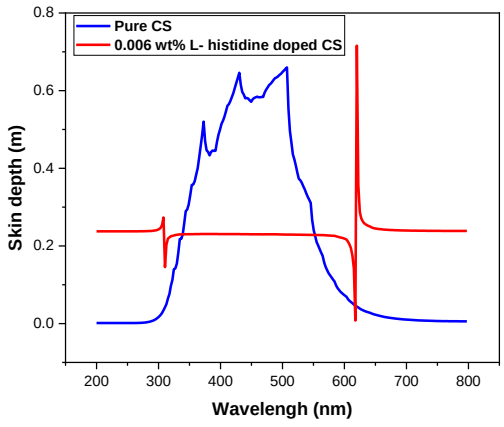

Fig. 11. Variation of skin depth as a function of wavelength of pure and doped CS crystals.

3.4 Micro hardness studies

Hardness and micro hardness are the two most authoritative parameters applied to describe the roughness of the material's surface. Hardness defines a material's ability to oppose twist that is determined by a synchronized test that computes the surface resistance to indentation [43, 44]. Micro hardness studies of the crystals yields information on strength, molecular bindings, yield strength, and elastic constants such as brittleness index and temperature of cracking of the materials [45-47]. Various factors such as Debye temperature, lattice energy, interatomic spacing, and heat of formation affect a material's hardness [48–50]. Measurement of hardness is a valuable non-critical method for finding out whether the crystal can be relevant to the manufacture of particular gadget. The Vicker's hardness number is calculated using the following equation

$$H_V = 1.8544 \frac{P}{d^2} \quad (8)$$

Here P is the applied load and d is the average diagonal indentation length. Fig. 12 and Fig. 13 indicate the deviation of Vicker's micro hardness number as a function of load for the pure and doped CS crystals respectively. From the graphs, it can be noted that the hardness number increases up to 100 g as the load increases which denotes reverse indentation size effect (RISE) of the material. Beyond 100 g, cracks appear which may be caused by the liberate of internal stresses. Higher hardness involves less cracking, breaking and waste during polishing, carving and grinding of crystal for the construction of NLO apparatus [51].

Mayer's law states the relationship between applied load P and the diagonal length d of the indenter as follows

$$P = Ad^n \quad (9)$$

where A is a constant and n implies the work hardening coefficient that was calculated from the slope of the plots connecting log d vs. log P indicated in Fig. 14 and Fig. 15 respectively. This signifies that the synthesized pure and doped CS single crystals belong to the type of soft materials. From the plots, the values of n are found to be 2.07 and 2.26 for the pure and doped CS crystals respectively. According to Onitsch, the values of n denote that the grown CS crystals are soft materials [52]. Therefore, the grown crystal can be utilized for the manufacture of optoelectronic appliances. Yield strength (σ_y) and elastic stiffness (C_{11}) are the most considerable factors for the design and fabrication of engineering tools. Yield strength is a measure of the smallest quantity of stress needed to oppose permanent deformation. The elastic stiffness constant designates the degree of bonding between adjacent atoms. It is expressed in terms of hardness number H_V. Fracture toughness (Kc) study can illustrate a material's capability to defy breakage in the existence of fracture. Toughness is depicted as a material's

capacity to oppose fracture. It is a significant factor to consider while choosing materials for applications where the load goes beyond the limit or yield point. Brittleness (B_i) takes place when a material cracks unexpectedly under stress, without any considerable elastic deformation or measurement alteration [53]. All these factors can be computed by using the following relations

$$\sigma_y = \frac{3-n}{2.9}\left(\frac{12.5\,(n-2)}{3-n}\right)^{n-2} H_V \quad (10)$$

$$K_C = \frac{P}{\beta C^{3/2}} \quad (11)$$

$$C_{11} = (H_V)^{7/4} \quad (12)$$

$$B_i = \frac{H_v}{K_c} \quad (13)$$

where β is the geometrical indentation factor that equals to 7 and C is the crack length [54]. The variation of yield strength σy, elastic stiffness C11, fracture toughness KC and brittleness index Bi as a function of load for pure and doped CS single crystals are exhibited in Fig. 16, Fig. 17, Fig. 18, Fig. 19, Fig. 20, Fig. 21, Fig. 22 and Fig. 23 respectively.

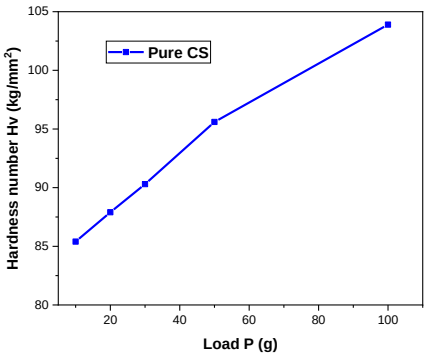

Fig. 12. Variation of hardness number as a function of load for pure CS crystal.

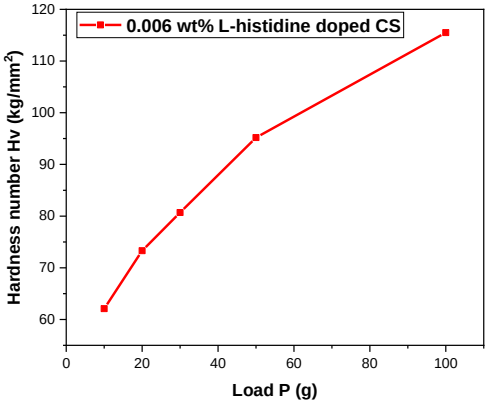

Fig. 13. Variation of hardness number as a function of load for doped CS crystal.

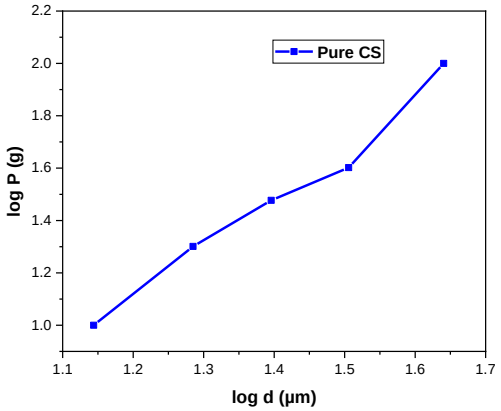

Fig. 14. Variation of log d against log P for pure CS crystal.

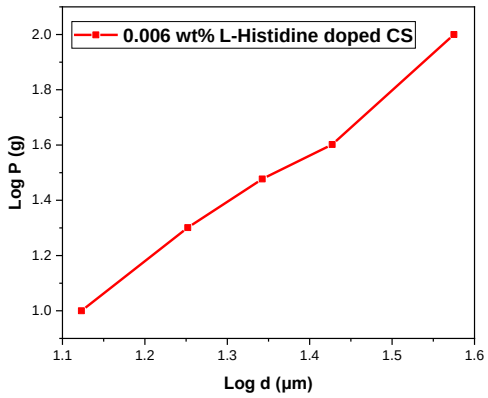

Fig. 15. Variation of log d against log P for doped CS crystal.

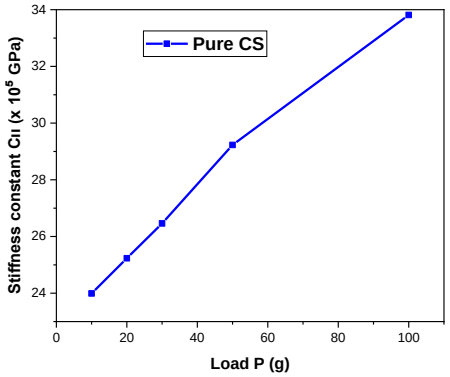

Fig. 18. Plot of Stiffness constant as a function of load for pure CS crystal.

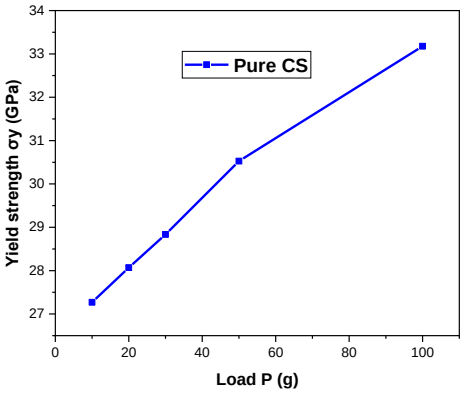

Fig. 16. Plot of Yield strength as a function of load for pure CS crystal.

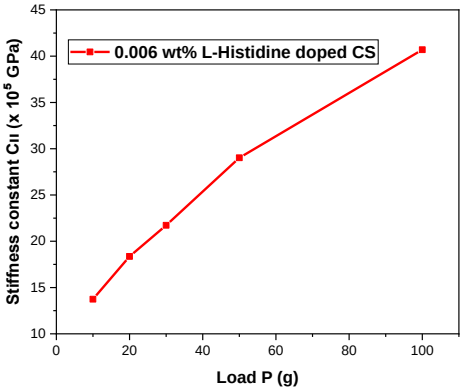

Fig. 19. Plot of Stiffness constant as a function of load for doped CS crystal.

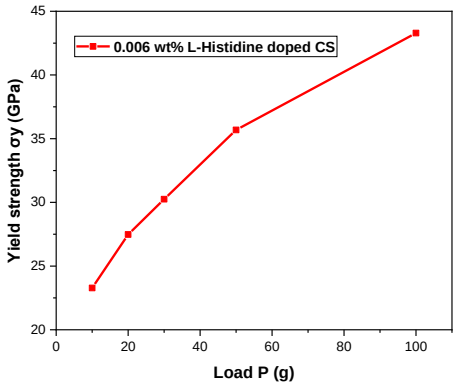

Fig. 17. Plot of Yield strength as a function of load for doped CS crystal.

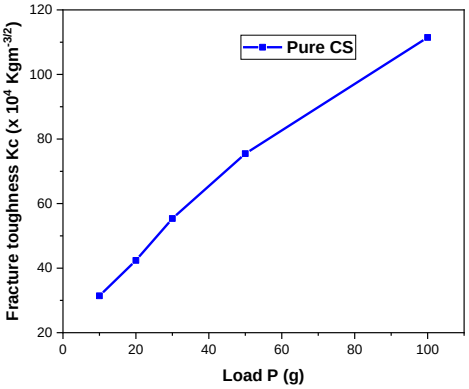

Fig. 20. Plot of Fracture toughness as a function of load for pure CS crystal.

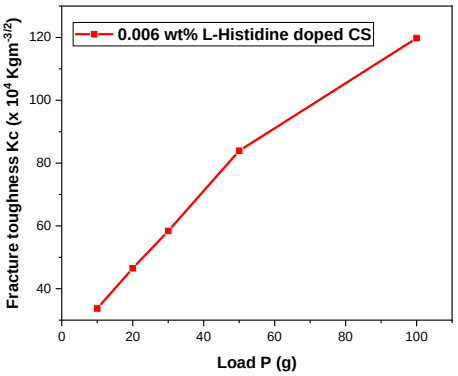

Fig. 21. Plot of Fracture toughness as a function of load for doped CS crystal.

Table 4. Mechanical parameters of pure CS crystal

Load P (g)	Vickers Hardness H_V (Kg/mm^2)	Yield strength σ_y (GPa)	Stiffness constant C_{11} (x10^5 GPa)	Fracture toughness K_C (x10^4 Kgm$^{-3/4}$)	Brittleness index Bi (m$^{-1/2}$)
10	85.4	27.2699	23.9912	31.42	2.718
20	87.9	28.0682	25.2337	42.39	2.0736
30	90.3	28.8346	26.4617	59.91	1.6308
50	95.6	30.527	29.2281	81.28	1.2667
100	103.9	33.1773	33.8125	111.47	0.9321

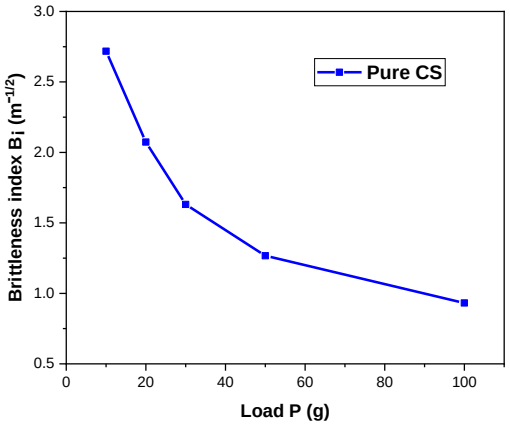

Fig. 22. Plot of Brittleness index as a function of load for pure CS crystal.

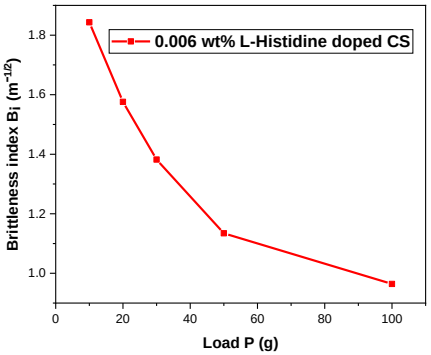

Fig. 23. Plot of Brittleness index as a function of load for doped CS crystal.

The attained values of yield strength, elastic stiffness, fracture toughness and brittleness index are specified in Table 4 and Table 5.

Table 5. Mechanical parameters of L-Histidine doped CS crystal

Load P (g)	Vickers Hardness H_V (Kg/mm^2)	Yield strength σ_y (GPa)	Stiffness constant C_{11} (x10^5 GPa)	Fracture toughness K_C (x10^4 Kgm$^{-3/4}$)	Brittleness index Bi (m$^{-1/2}$)
10	62.1	23.2766	13.7376	33.69	1.8433
20	73.3	27.4747	18.3625	46.505	1.576
30	80.7	30.2484	21.7284	58.39	1.3821
50	95.2	35.6833	29.0145	83.917	1.1345
100	115.5	43.2923	40.6929	119.777	0.9643

3.5 Nonlinear optical studies

Kurtz-Perry powder SHG has been carried out in order to examine the efficient laser frequency doubling performance of pure and doped CS single crystals [55, 56]. In this analysis, perfectly synthesized pure and doped CS crystals were delicately minced and enclosed firmly in a micro-capillary tube of standard uniform bore of 1.5 diameters. The first harmonic output of *1064 nm* with pulse width of *6 ns* and repetition rate

of *10 Hz* of *Q - switched High Energy Nd:YAG Laser* (QUANTA RAY Model LAB – 170 - 10) was applied to light up the tasters. After passing crystal radiations of 1064 nm, the output second harmonic radiations (532 nm) were focused by a lens and detected by a photomultiplier tube [57]. The powdered form of KDP was utilized as the reference material and the output energy of the synthesized crystals were compared with the output energy of KDP. The energy level should not cause any chemical decomposition of the samples. Hence the input laser energy of the incident on the capillary tube was chosen to be *0.701 J* [58]. The output energy of the input KDP was recognized as *8.94 mJ*. It is detected from the analysis that there is no emission of green light from the samples. Hence it is concluded that the synthesized CS crystals yield to zero second order susceptibility coefficient and the grown CS crystals have *Centro symmetric* crystal structure [59].

4. Conclusion

Optically clear, single crystals of pure and L-histidine doped CS single crystals are suitably synthesized by slow solvent evaporation method. The PXRD studies confirm the triclinic structure of the crystals. The vibration modes of functional groups were recognized using FTIR spectroscopic analysis. UV– Vis NIR studies emphasize the excellent transparency of the crystal in the whole visible region. The Micro hardness study exposes the crystals are soft in nature. SHG test reveals that the grown crystals have Centro symmetric crystal structure. The (CSP) crystals can be utilized as optical band pass filters. In an overall view, the compound reported herein can be proposed as a potent material for nonlinear, optical, biomedical and photonic applications.

Acknowledgements

The authors are grateful to SAIF, Pondicherry University, Crescent Institute of Science and Technology, Chennai, M.D.T. Hindu College, Tirunelveli for yielding outstanding instrumentation facilities.

Conflict of interest: The authors declare that they have no conflict of interest.

References

1. G.A. Jeffrey, W. Saenger, Hydrogen bonding in Biological structures, Springer-Verlag, Berlin, 1991.

2. A.H. Reshak, S. Auluck, D. Stys, I.V. Kityk, H. Kamarudin, J. Berdowski, Z. Tylczynski, 'Dispersion of linear and nonlinear optical susceptibilities for amino acid 2-aminopropanoic CH3CH(NH2)COOH single crystals: experimental and theoretical investigations', *J. Mater. Chem.* 21 (2011) 17219–17228, https://doi.org/ 10.1039/C0CP01601B.

3. M. Rajkumar, A. Chandramohan, 'Synthesis, structural, thermal and mechanical properties of 1, 10- phenanthrolinium-3-carboxy-4-hydroxy benzene sulfonate crystal: an efficient SHG

material with a high laser damage threshold for NLO applications', *Mater. Lett.* 199 (2017) 53–56, https://doi.org/10.1016/j.matlet.2017.04.049.

4. S. Ramteke, M. Anis, M. Baig, H. Algarni, G. Muley, 'Optimizing optical traits of ammonium zinc sulphate hydrate crystal exploiting Nd+ for photonic device applications', *Optik* 197 (2019), 163219, https://doi.org/10.1016/j.ijleo.2019.163219.

5. R.W. Boyd, *Nonlinear Optics*, Academic Press, San Diego, 1992.

6. I. Sharma, and A.S. Hassanien, *J. Non Cryst. Solids.* 548, 120326(2020).

7. P. Gunter, *Nonlinear Optical Effects and Materials* (Berlin:Springer-verlag, 2000).

8. S. Sun, and N.S. Sariciftci, *Organic Photovoltaics Mechanisms, Materials and Devices* (USA: CRC Press Taylor and Francis group, 2005).

9. I.M. El-Radaf, H.Y.S. Al-Zahrani, and A.S. Hassanien, *J. Mater. Sci. Mater. Electron.* 31, 8336 (2020).

10. A.S. Hassanien, I. Sharma, and K.A. Aly, *Physica B Condens. Matter.* 613, 412985 (2021).

11. G.R. Kumar, S.G. Raj, R. Mohan, R. Jayavel, 'Influence of isoelectric pH on the growth linear and nonlinear optical and dielectric properties of L-threonine single crystals', Cryst. *Growth Des.* 6 (2006) 1308–1310, https://doi.org/10.1021/cg050438g.

12. S. Suresh, A. Ramanand, D. Jayaraman, P. Mani, 'Review on theoretical aspect of nonlinear optics', *Rev. Adv. Mater. Sci.* 30 (2012) 175–183.

13. S.Aruna, G.Bhagavannarayana, P. Sagayaraj, *J. Crystal Growth* 304, (**2007**) 184-190.

14. S. N. Jayanthi , A.R. Prabhakaran, D. Subashini, K. Thamizharasan, 'Crystallization and Characterization of NLO active glycine copper sulphate crystal', *Chalcogenide Letters*, 11 (2014) 241-247.

15. S.P. Ramteke , S.M. Azhar , G.G. Mule, 'Growth and optimization of optical traits of copper sulphate crystal exploiting L-ascorbic acid for photonic device applications', *Chinese J. of Phy.*, S0577-9073(20)30094-0, DOI: https://doi.org/10.1016/j.cjph.2020.04.006.

16. R. Thilagavathi, P. Selvarajan, V. Vasantha Kumari, 'Growth, optical, thermal and mechanical properties of glysine copper sulphate single crystal', *Inter. J. of advance sci. and tech. research*, Iss. 2, vol. 6, Dec. 2012. ISSN 2249-9954.

17. Tapash Chandra Paul, Jiban Podder, 'Synthesis and characterization of Zn-incorporated TiO_2 thin films: impact of crystallite size on X-ray line broadening and band gap tuning', *Applied Physics A* (2019) 125:818, https://doi.org/10.1007/s00339-019-3112-9.

18. JCPDS file card no:77-1900.

19. T. Suthan, N.P. Rajesh, 'Growth and characterization of organic material 4-nitrobenzaldehyde single crystal using modified

vertical Bridgman technique', *J. of Cry. Growth*, 312 (2010) 3156–3160.

20. T. Prasanyaa and M. Haris, 'Growth and characterization of semiorganic NLO L-arginine trifluoroacetate (LATF) added KDP single crystals', *Archives of Physics Research*, 2 (2011) 60-66.

21. Fei Lu, Hai-Shui Wang, Xinmei Zhao, Yukihiro Ozaki, "Nucleation and growth of CuSO4.5H2O crystals on the liquid states tearic acid Langmuir-Blodgettfilm", Journal of Cry. Growth, Vol. 310, pp. 4652-4655, (2008). DOI : ttp://dx.doi.org/10.24237/djps.1303.291C.

22. S. A. Moggach, D. R. Allan, C. A. Morrison, S. Parsons, L. Sawye, 'Effect of Pressure on the crystal structure of LSerine- I and crystal structure of L-Serine-II at 5.4 Gpa', *Acta Crystalographica B*, vol. 61, part 1, pp. 58–68, 2005.

23. Chandrashekhar M. Bhambere, N. G. Durge, 'Study on structural, spectral, and optical properties of Copper Sulphate doped LMethionine Crystal', *JETIR*, July 2021, Vol. 8, Issue 7

24. Redrothu Hanumantharao, S. Kalainathan, 'Crystal growth and optical studies on a semi organic nonlinear optical material for laser blue-green generation', *Optik* (2012), http://dx.doi.org/10.1016/j.ijleo.2012.06.098.

25. M.R. Jagadeesh, H. M. Suresh Kumar, R. Ananda Kumari**, '**Growth and characterization of an organic NLO crystal: L-alanine-2-furoic acid', *Arch. of App. Sci. Res.*, 6 (2014) 188-197.

26. Richard A. Nyquist and Ronald O. Kagel, (1971), 'Infrared Spectra of Inorganic Compounds', *Academic Press*, INC, New York.

27. S. M. Delphine, R. K. Priya, T. L. A. Thai and S. Ajitha, (2014), *Scholars Research Library*, 6, 4, 157-161.

28. Briyan C. Smith, 'Infrared Spectral Interpretation-A systematic Approach', CRC Press (1999), New York.

29. F. A. Miller and C. H. Wilkins, 'Infrared Spectra and Characteristic Frequencies of Inorganic Ions', *Analytical Chemistry*, 24 (1952) 1253-1294.

30. J. Berger, (1976), J. of Raman Spectroscopy, 5, 103-114.

31. Nabeel A. Bakr, Tariq A. Al- Dhahir, Saja B. Mohammad, 'Growth of Copper Sulfate Pentahydrate Single Crystals by Slow Evaporation Technique', *J. of Adv. in Phy.*, Vol. 1 3, No. 2. DOI: 10.24297/jap.v13i2.5963.

32. T. Suthan, P.V. Dhanaraj, N.P. Rajesh, C.K. Mahadevan, G.Bhagavannarayana, *Cryst. Eng. Comm.* 13, 4018 (2011).

33. T. Suthan, N.P. Rajesh, C.K. Mahadevan, D. Sajan, and G. Bhagavannarayana, *Mater. Chem. Phys.* 130, 915 (2011).

34. A.S. Hassanien, I.M. El Radaf, A.A. Akl, *J. Alloys Compd.* 849, 156718 (2020).

35. V. Revathi Ambika, D. Shalini, R. Usha, N. Hema, S. Athimoolam, D. Jayalakshmi. 'Synthesis, growth, optical, spectral, thermal and dielectric studies of a new nonlinear optical material: l-proline 2,4-dichlorobenzoic acid single crystal', *J. Mater. Sci: Mater. Electron.*

(2017). https://doi.org/10.1007/s10854-017-7273-z.

36. M. Prakash, D. Geetha, M. Lydia Caroline, 'Crystal growth and characterization of L-phenylalaninium trichloroacetate— A new organic nonlinear optical material', *Physica B*, 406 (2011) 2621–2625, 10.1016/j.physb.2011.04.002.

37. S. Prince, T. Suthan, C. Gnanasambandam, N. P. Rajesh, 'Growth and characterization of organic 4-methyl-2-nitroaniline single crystals for nonlinear optical applications', *J. Mater Sci: Mater Electron*, https://doi.org/10.1007/s10854-022-07772-2.

38. K. Kumar, K. Ramamoorthy, P.M. Koinkar, R. Chandramohan, K. Sankaranarayanan, 'A novel in situ synthesis and growth of ZnAl2O4 thin films', *J. Cryst. Growth*, 289, 405–407 (2006). https://doi.org/10.1016/j.jcrysgro.2005.11.007

39. S. Senthilkumar, R. Manimekalai, 'Growth and evaluation of linear optical, nonlinear optical, mechanical and thermal properties of a novel bio-organic chlorophyll-b of Ficus religiosa added ammonium dihydrogen phosphate optical single crystal', *J. Optik* 212, 164679 (2020). https://doi.org/10.1016/j.ijleo.2020.164679.

40. P. Sangeetha, P. Jayaprakash, M. Nageshwari, C.S. Rathika Thaya Kumari Sutha, 'Growth and characterization of an efficient new NLO single crystal L-phenylalanine D-methionine for frequency conversion and optoelectronic applications', *J. Phys. B* 525, 164–174 (2017). https://doi.org/10.1016/j.physb.2017.08.037.

41. P. Jayaprakash, M. Peer Mohamed, P. Krishnan, M. Nageshwari, G. Mani, M. Lydia Caroline, 'Growth, spectral, thermal, laser damage threshold, microhardness, dielectric, linear and nonlinear optical properties of an organic single crystal: L-phenylalanine DL-mandelic acid', *J. Phys. B* 503, 25–31 (2016). https://doi.org/10.1016/j.physb.2016.09.010.

42. S. Prince, T. Suthan, C. Gnanasambandam, 'Growth and Characterization of Organic 2,4-Dinitroaniline Single Crystals for Optical Applications', *J. of Electronic Materials*, https://doi.org/10.1007/s11664-022-09428-7.

43. W. Gwidon Stachowiak, W. Andrew Batchelor, B. Grazyna Stachowiak, J. Tribol. Ind. 44 (2004) 13–23, https://doi.org/10.1016/S0167-8922(04)80018-X.

44. Peter Smith, The Fundamentals of Piping Design, Gulf publishing Company, Texas, 2007.

45. K. Li, X. Wang, D. Xue, 'A simple method of Hardness prediction of transition metal compounds', *J. Mater. Focus*. 1, 142–148 (2012). https://doi.org/10.1166/mat.2012.1012

46. K. Li, P. Yang, L. Niu, D. Xue, 'Group electro negativity for prediction of materials hardness', *J. Phys. Chem. A*, 116, 6911–6916 (2012). https://doi.org/10.1021/jp3032258

47. K. Li, X. Wang, F. Zhang, D. Xue, 'Electro negativity identification of novel super hard materials', *J. Phys. Rev. Lett.* 100, 235504 (2008),

https://doi.org/10.1103/PhysRevLett.100.235504.

48. C.C. Desai, J.L. Raj, 'Microhardness studies of SnI_2 and SnI_4 single crystals', *Bull. Mater. Sci.* 5 (1983) 453–457, https://doi.org/10.1007/BF02743924.

49. V. Sangeetha, K. Gayathri, P. Krishnan, N. Sivakumar, N. Kanagathara, G. Anbalagan, 'Growth, optical, thermal, dielectric and microhardness characterization of melaminium bis (trifluoroacetate) trihydrate single crystal', *J. Cryst. Growth* 389 (2014) 30–38, https://doi.org/10.1016/j.jcrysgro.2013.11.026.

50. B.W. Mott, Micro indentation Hardness Testing, Butterworths, London, 1956.

51. M. Anis, G.G. Muley, M.I. Baig, G. Rabbani, H.A. Ghramh, S.P. Ramteke, 'Doping effect of Ni2? on structural, UV-visible, SHG efficiency, dielectric and microhardness traits of KH2PO4 (KDP) crystal', *J. Optik*, (2018). https://doi.org/10.1016/j.ijleo.2018.10.061

52. E.M. Onitsch, 'Systematic metallographic and mineralogic structures. Mikroskopia', 2, 131–138 (1947).

53. D. Abila Darling, S.E. Joema, 'Investigation of structural, mechanical, optical, thermal and in vitro antimicrobial study of L-phenylalaninium formate single crystals', *J. Mater. Sci.: Mater. Electron.* 32 (2021) 9087–9105, https://doi.org/10.1007/s10854-021-05577-3.

54. D. Abila Darling, S.E. Joema, P. Reena, 'Enhanced antimicrobial activity and physicochemical properties of an organic nonlinear optical crystal: L-tryptophan L-tryptophanium bromide (LTTB) for biomedical applications', *Chemical Data Collections*, 38 (2022) 100839, https://doi.org/10.1016/j.cdc.2022.100839.

55. T.T. Perry, S.K. Kurtz, *J. of Applied Phy*. 39 (1968) 3798–3812.

56. R. Hanumanthrao, S. Kalainathan, Spectrochim. *Acta A* 94 (2012) 78–83.

57. D. Abila Darling, S.E. Joema, P. Reena, 'Enhanced antimicrobial activity and physicochemical properties of an organic nonlinear optical crystal: L-tryptophan L-tryptophanium bromide (LTTB) for biomedical applications', *Chemical Data Collections* 38 (2022) 100839, https://doi.org/10.1016/j.cdc.2022.100839.

58. R. Hanumantharao, S. Kalainathan, G. Bhagavannarayana, U. Madhusoodanan, 'An extensive investigation on nucleation, growth parameters, crystalline perfection, spectroscopy, thermal, optical, microhardness, dielectric and SHG studies on potential NLO crystal – Ammonium Hydrogen L-tartarte', *Spectrochimica Acta Part A: Molecular and Biomolecular Spectroscopy*, 103 (2013) 388–399. https://doi.org/10.1016/j.saa.2012.10.044.

59. R Thilagavathi. P. Selva Rajan, V. Vasantha Kumari, 'Growth, optical, thermal and mechanical properties of glycine copper sulphate single crystal', *Inter. J. Advan. Scien. And Tech. Research*, issue 2, vol. 6, Dec. 2012.

Optics and Photonics, 10(1), 43. doi:10.1364/aop.10.000043

[53] AlQatari, F., Sajjad, M., Lin, R., Li, K. H., Schwingenschlogl, U., & Li, X. (2018). Optical properties of BalN and BGaN for applications in latticematched UV optical structures. arXiv preprint arXiv:1803.10011.